Supporting Information

Boosting Lithium Storage Capability of Li^+-Conductor $LiInGeO_4$ through Intrinsic and Extrinsic Conductivity Optimization

Haipeng Wang[a,1], Ran Niu[a,1], Shuoyu Wang[a], Zedong Li[a], Hongming Zhang[a], Pengfei Hou[a], Xinxin Wang[a], Jingjing Chen[a], Chenlong Dong[a,*] and Zhiyong Mao[a,*]

[a] Tianjin Key Laboratory for Photoelectric Materials and Devices, Key Laboratory of Display Materials and Photoelectric Devices, School of Materials Science and Engineering, Tianjin University of Technology, Tianjin 300384, PR China

[1] These authors contributed equally to this work.

* Corresponding authors. *E-mail address*: mzhy1984@163.com (Prof. Zhiyong Mao), dongchenlong@email.tjut.edu.cn (Prof. Chenlong Dong)

Experimental Section

Materials

Li_2CO_3 (99.9%), In_2O_3 (99.99%), GeO_2 (99.99%), and RuO_2 (99.9%) were purchased from Macklin Co., Ltd. Acetylene black, carbon nanotubes and graphene was purchased from Shenzhen Kejing star technology Co., Ltd. All of materials were used without further purification.

Material Synthesis

Preparation of $LiInGeO_4$ and $LiInGe_{0.9}Ru_{0.1}O_4$: Both $LiInGeO_4$ (named as LIGO) and $LiInGe_{0.9}Ru_{0.1}O_4$ (LIGRO) powders were synthesized using a conventional high-temperature solid-state reaction method. For $LiInGeO_4$, stoichiometric amounts of Li_2CO_3, In_2O_3 and GeO_2 were weighed according to a molar ratio of 1:1:2, with an additional 5 *wt.*% excess of Li_2CO_3 to compensate for potential lithium loss at high temperature. The raw materials were thoroughly mixed and homogenized using an agate mortar and pestle. The mixture was subsequently annealed in a muffle furnace at 1000°C for 6 h. For $LiInGe_{0.9}Ru_{0.1}O_4$, the reactants including Li_2CO_3, In_2O_3, GeO_2, and RuO_2 were weighed in a molar ratio of 1:1:1.8:0.2 with 5 *wt.*% excess of Li_2CO_3. The mixed powders were similarly heated at 1000°C for 6 h in muffle furnace.

Preparation of carbon-composite anode materials: The as-synthesized LIGO powders were separately mixed with acetylene black (AB), graphene (G) and carbon nanotubes (CNTs) in a mass ratio of 7:2 using high-energy ball milling in a ZrO_2 jar at 1400 rpm for 2 h, and the resulting products were marked as LIGO/AB, LIGO/G and LIGO/CNTs. Similarly, $LiInGe_{0.9}Ru_{0.1}O_4$ was ball-milled with G to prepare the LIGRO/G composite.

Material Characterizations

The phase structure of the synthesized samples was characterized by X-ray diffraction (XRD) on an ARL EQUINOX 3000 diffractometer (Thermo Fisher Scientific) using Cu Kα radiation (λ = 1.5418 Å) and the data was collected in the 2θ range of 10° to 70°. Morphological analyses were performed using an ultra-high resolution scanning electron microscope (Verios 460 L, FEI), operating at an acceleration voltage of 10 kV. The microstructure, crystal and composition were further

investigated by transmission electron microscopy (TEM) using a JEM-F200 instrument (JEOL) equipped with high-angle annular dark-field scanning TEM (HAADF-STEM) and energy-dispersive X-ray spectroscopy (EDX) system. The chemical states of elements were investigated by X-ray photoelectron spectroscopy (XPS) on an Axis Ultra spectrometer (Kratos Analytical) with Al Kα radiation ($h\nu$ = 1486.7 eV). All binding energies were calibrated relative to the adventitious C 1*s* peak at 284.8 eV. Molecular structure and vibrational information were acquired by Raman spectroscopy (HORIBA JOBIN YVON S.A.S., France). Optical absorption properties were examined using ultraviolet-visible (UV-Vis) spectroscopy on a TU-1901 spectrometer (China) equipped with a Φ60 mm integrating sphere. The electronic conductivity was obtained by powder material resistivity tester (ST2742B-SD) *via* four-probe method.

Electrochemical Measurements

The electrode slurry was prepared by homogeneously mixing the active material, acetylene black, and polyvinylidene fluoride (PVDF) in a mass ratio of 8:1:1 using N-methyl-2-pyrrolidone (NMP) as the solvent. This slurry was uniformly deposited onto a Cu current collector using a doctor-blade coating technique, followed by drying in a vacuum oven at 80°C for 12 h. The dried electrodes were then punched into Φ 12 mm circular discs for battery assembly. Coin-type CR2016 cells were assembled in an argon-filled glove box, where the concentrations of moisture and oxygen were maintained below 0.01 ppm. A lithium metal foil was employed as both the counter and reference electrode. A glass fiber membrane (Whatman) served as the separator. The electrolyte was 1 M $LiPF_6$ dissolved in a mixture of ethyl carbonate (EC) and diethyl carbonate (DEC) (1:1, *w/w*) with 10.0% fluoroethylene carbonate (FEC) and 1.0% vinylene carbonate (VC) as functional additives. The mass loading of the active material was controlled at approximately 1.5 mg cm^{-2}. Galvanostatic charge/discharge profiling and rate capability assessments were conducted using a LAND CT2001A battery test system, operating within a voltage window of 0.01–3.0 V (*vs.* Li/Li^+) at 25°C. Cyclic voltammetry (CV) measurements were performed on a CHI760E electrochemical workstation with scan rates varying from 0.1 to 5 mV s^{-1} over the identical potential range. Electrochemical impedance spectroscopy (EIS) was carried

out with an amplitude of 5 mV over a frequency range from 100 kHz to 0.01 Hz.

The Li^+ diffusion coefficients (D_{Li}) can be calculated based on the following equation:

$$D_{Li} = \frac{R^2T^2}{2\sigma^2A^2C^2n^4F^4}$$

$$Z' = R_S + R_{ct} + \sigma\omega^{-1/2}$$

Where *n* is electron-transfer number, *F* is Faraday constant, *C* is Li^+ concentration, *A* is the electrode area, *R* is gas constant and *T* is temperature.

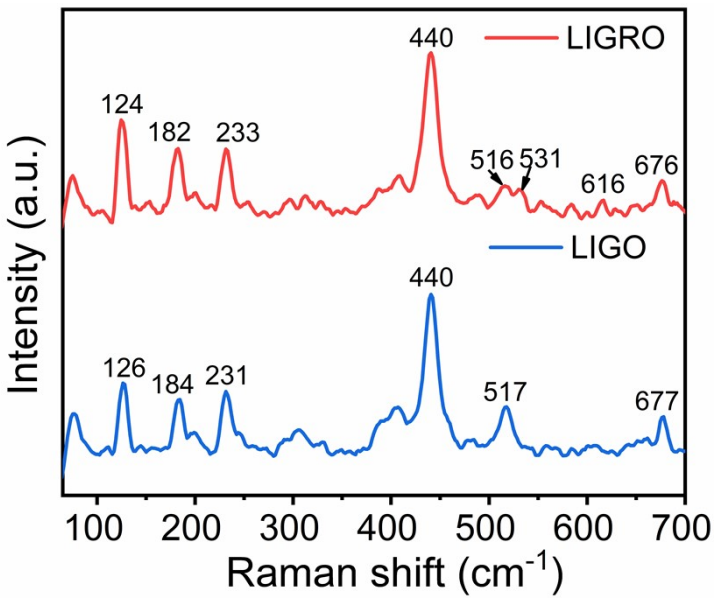

Figure S1. Raman spectra of LIGO and LIGRO.

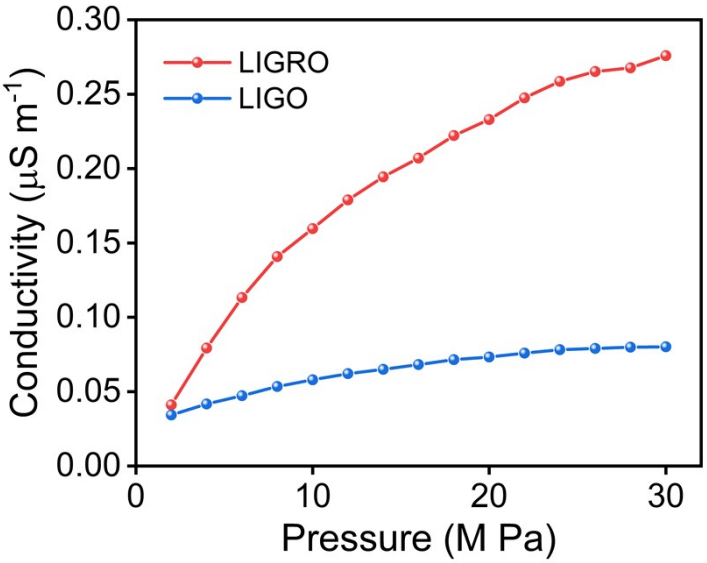

Figure S2. Electronic conductivity measurements of LIGO and LIGRO.

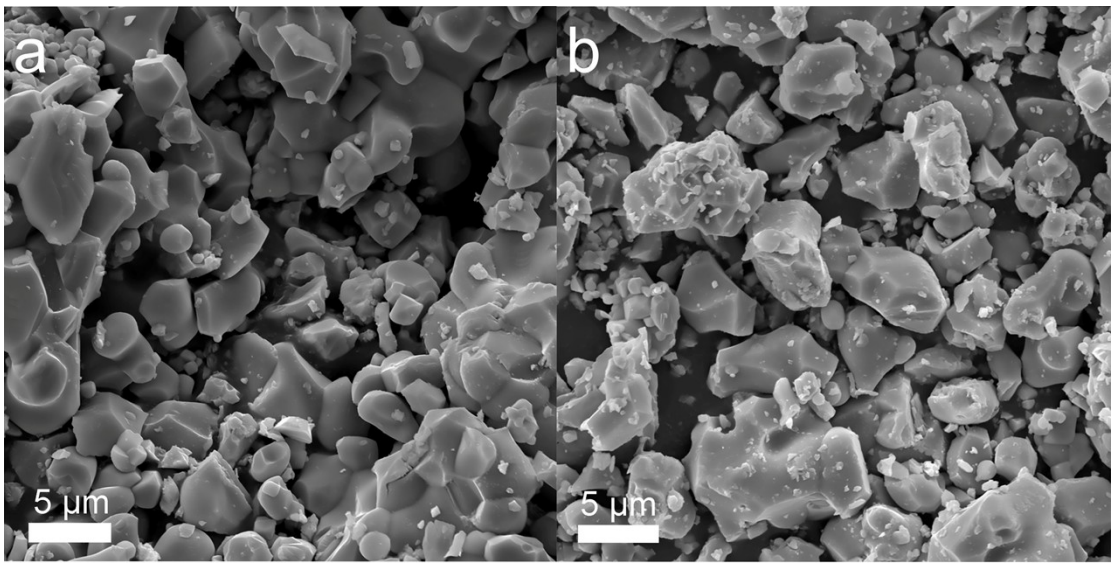

Figure S3. SEM images of (a) LIGO and (b) LIGRO.

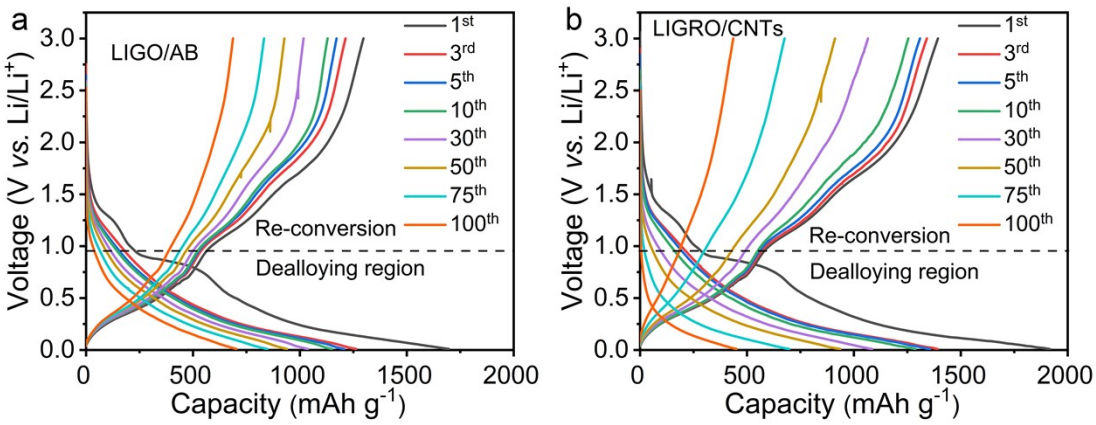

Figure S4. GCD curves of (a) LIGO/AB and (b) LIGO/CNTs.

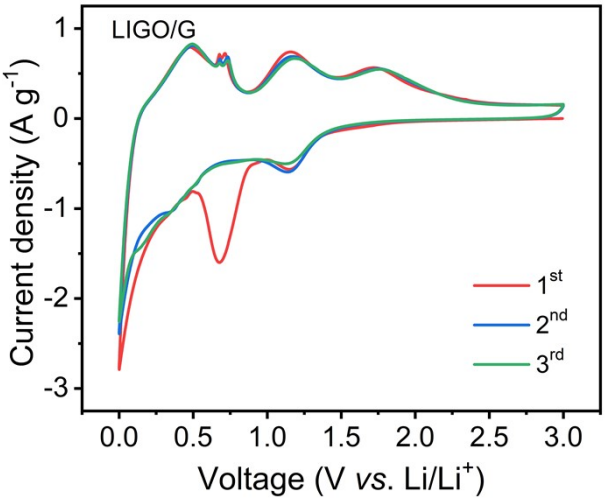

Figure S5. CV curves of LIGO/G.

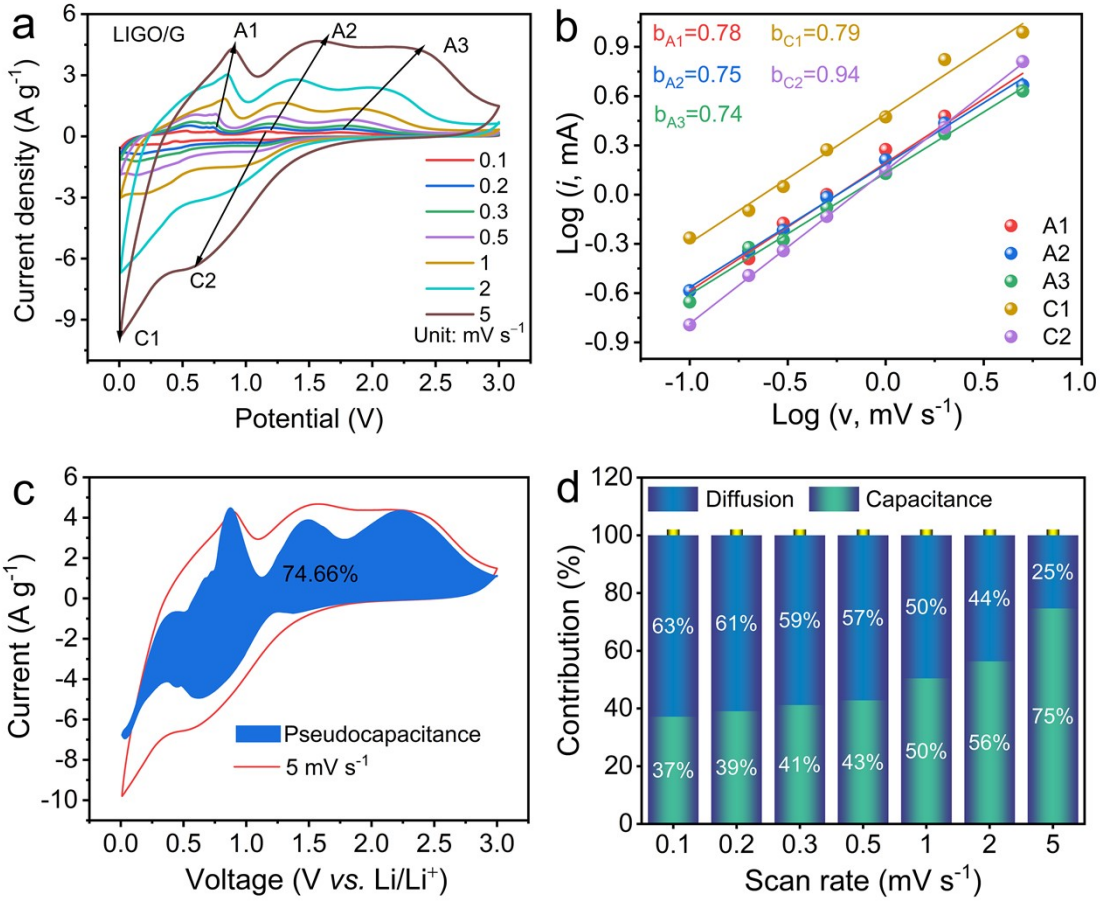

Figure S6. (a) CV curves at different scan rates, (b) linear relationship between the log(*i*) and log(*v*), (c) pseudocapacitance contribution at 5 mV s^{-1} and (d) pseudocapacitance and diffusion contributions at different scan rates of LIGO/G.

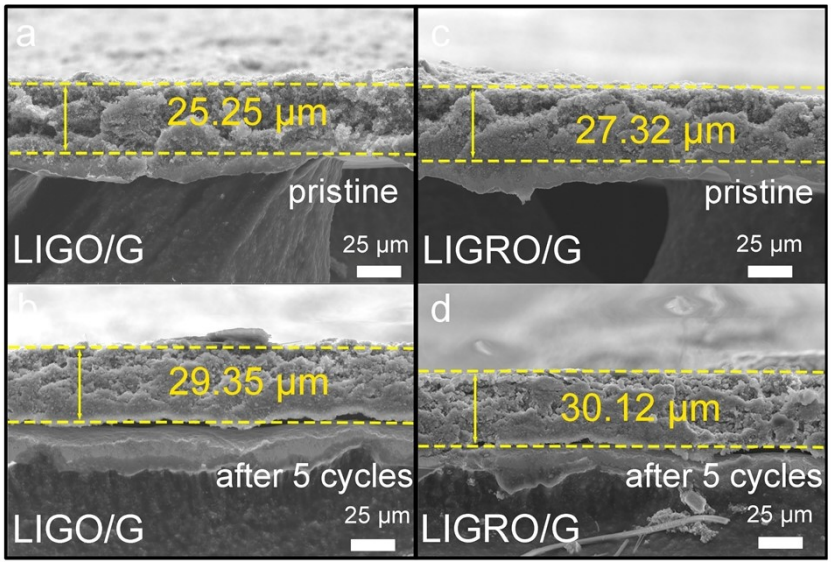

Figure S7. Ex situ cross-sectional SEM images of (a, b) LIGO/G and (c, d) LIGRO/G electrodes before and after 5 cycles.

Table S1. Electrochemical performance comparison of LIGRO/G with representative Li^+ conductor-derived anodes.

Materials	Capacity at low current (mAh g^{-1}@A g^{-1})	Capacity at high current (mAh g^{-1}@A g^{-1})	Capacity (mAh g^{-1})@cycles@current (A g^{-1})	Ref.
$Rb_4Li_2TiOGe_4O_{12}$	564@0.1	88@2.5	472@160@0.1	1
Li_2TiGeO_5	639@0.1	287@5	406@600@1	2
$Li_3V_2(PO_4)_3$	91@0.1	–	72.8@100@0.1	3
$La_{0.5}Li_{0.5}TiO_3$	449@0.02	100@2	79@3000@2	4
$Li_{1.5}Al_{0.5}Ge_{1.5}(PO_4)_3$	340@0.15	200@1.5	~240@100@0.15	5
$Li_2ZnTi_3O_8$@Li_3PO_4	296.4@0.1	154.7@10	133.4@200@5	6
$LiNbGeO_5$@C	720.8@0.1	512@1	135@5000@10	7
$LiInGe_{0.9}Ru_{0.1}O_4$/G	1266.5@0.1	600.8@5 412.8@10	1058.8@100@0.1 1043.2@200@1 574.2@300@5	This work

References

1. Tang et al. $Rb_4Li_2TiOGe_4O_{12}$: a novel high-performance titanyl germanate anode for Li-ion batteries. *J. Mater. Chem. A* 11 (2023): 7170-7178.

2. Liu et al. Lithium ion storage in lithium titanium germanate. *Nano Energy* 66 (2019): 104094.

3. Satish et al. Carbon-coated $Li_3V_2(PO_4)_3$ as insertion type electrode for lithium-ion hybrid electrochemical capacitors: An evaluation of anode and cathodic performance. *J. Power Sources* 281 (2015): 310-317.

4. Zhang et al. Lithium lanthanum titanate perovskite as an anode for lithium ion batteries. Nat. Commun. 11 (2020): 3490.

5. Feng et al. Lithium storage capability of lithium ion conductor $Li_{1.5}Al_{0.5}Ge_{1.5}(PO_4)_3$. *J. Alloys Compds.* 501 (2010): 255-258.

6. Liu et al. A Li_3PO_4 coating strategy to enhance the Li-ion transport properties of $Li_2ZnTi_3O_8$ anode material for Lithium-ion Battery. *Electrochim. Acta* 447 (2023): 142151.

7. Cao et al. A new germanium-based anode material with high stability for lithium-ion batteries. *ACS Sustain. Chem. Eng.* 9 (2021): 11883-11890.